Supplement Material

Reagents

If not otherwise specified, the concentrations of chemicals used were as follows: H_2O_2 and $ONOO^-$ (both 100 μM), $ZnCl_2$ (0.1-1.0 μM + 4 μM pyrithione), $ZnCl_2$ (10 and 20 μM in 40 and 100 mM KCl, respectively), TPEN (15-50 μM), membrane permeable ester GSH (2 mM), NAC (10 mM), dithiothreitol (DTT; 1 mM), LiCl (10 mM), SB216763 (SB21; 5 μM); MG132, flavonoids (baicalein, luteolin and fisetin), U0126, and MK886 (all 10 μM), PFT-α (20 μM), PD98059 (30 μM), diazoxide (50 μM); CsA and FCCP (both 1 μM); z-DEVD.fmk and z-VAD.fmk (both 100 μM), MnTBAP (0.2 mM).

MnTBAP, U0126 and MG132 were obtained from Calbiochem (San Diego, CA). PFT-α was purchased from BioVision (Mountain View, CA). Both $ONOO^-$ and PD98059 were from Cayman (Ann Arbor, MI). SB21, TPEN, flavonoids and all other chemicals were purchased from Sigma (St. Louis, MO). All fluorescent indicators were purchased from Molecular Probes (Eugene, OR). The terminal deoxynucleotidyl transferase-mediated dUTP nick end labeling (TUNEL) kit was purchased from Roche Molecular Biochemicals (Mannheim, Germany).

Anti-rabbit Noxa antibody was from Imgenex (San Diego, CA). Antibodies against cleaved caspase-3 (Aap175), PARP and monoclonal phospho-GSK-3β (p-Ser9) were purchased from Cell Signaling Technology (Beverly, MA). Antibody against cleaved caspase-3 (Aap175) was from GeneTex (Irrine, CA). Anti-phospho-GSK-3α/β (p-Tyr279)/(p-Tyr216) and anti-rat cytC monoclonal antibodies were purchased from Epitomics (Burlingame, CA) and Promega (Madison, WI), respectively. Anti-Mcl-1, anti-phospho-ERK1/2 and anti-ERK1/2 antibodies were from Santa Cruz Biotechnology (Santa Cruz, CA). Anti-p53 and anti-α-tubulin antibodies were from BioVision (Mountain View, CA) and Sigma (St. Louis, MO), respectively. All siRNAs, including siGSK-3β, sip53, siNoxa, siMcl-1, and si12/15-LOX, were obtained from Dharmacon as the

siGENOME SMARTpool reagents, except for scrambled siRNA, si12-LOX, siNFκB, siHIF1α, and the transfection reagent siPORT *NeoFX* were from Ambion (Austin, TX).

Protocols for simulating I/R in neonatal cardiomyocytes or I/R in adult rat hearts

A. Cultured neonatal ventricular myocytes

Cardiomyocytes were placed in a sealed chamber connected to a pump providing rapid changes of perfusate buffers and maintained at 37°C. Cells were stabilized with O_2 (21%)-Tyrode solution for 10 min, then were switched to hypoxia solution (100% N_2-saturated Tyrode solution) for 30-40 min. The reoxygenation (reperfusion) period was 4 hr in O_2-Tyrode solution.

B. Isolated adult rat hearts

Adult male Wistar rats (250-300 g) were anesthetized with a mixture of pentobarbital (50 mg/kg) and heparin (300 U/kg) and the heart rapidly removed. I/R was performed at a constant flow-rate of 11 ml/min with Krebs–Henseleit buffer (KHB) containing (in mM) NaCl 118, $NaHCO_3$ 25, KCl 4.8, KH_2PO_4 1.2, $MgSO_4$ 1.2, glucose 11 and $CaCl_2$ 1.2.[1] After 10 min stabilization, the hearts were subjected to 30 min of global ischemia by halting perfusion, followed by 2 hr of reperfusion with KHB gassed with 95% O_2/5% CO_2 at 37^{o}C (pH 7.4). The infarcted myocardium was measured by triphenyltetrazolium chloride staining and quantified using ImageQuant v5.0 (Molecular Dynamics).

Time-lapse confocal microscopy in live cardiomyocytes

A. Simultaneous measurement of intracellular/nuclear $[O_2^{-\bullet}]_i$ and $[Zn^{2+}]_i$ changes in triple-loaded myocytes

FluoZin-3 AM (5 μM, green fluorescence, 488 nm excitation/510 nm emission; band pass, BP; Kd for Zn^{2+} = 15 nM) and a mitochondrial marker MitoTracker Green (MTG; 200 nM, green fluorescence, 488/510 nm; arrowhead in Fig. 1A) were co-loaded with MitoSox Red (4 μM, red fluorescence; 568/630 nm; BP).[2] MitoSox Red is a cell-permeating selective $O_2^{-\bullet}{}_i$ indicator, which is readily oxidized by $O_2^{-\bullet}{}_i$. The oxidation product of MitoSox Red

becomes highly red fluorescent upon binding to DNA. Since the nuclear membrane does not represent a barrier to cytosolic ion movement,[3,4] averaging the fluorescent signal over a small nuclear optical section free of organelles, including endoplasmic reticulum and mitochondria (see labeled 'N' in the last frame in Fig. 1A), allows the simultaneous monitoring of dynamic changes in the $[O_2^{-\bullet}]_i$ (red fluorescence) and $[Zn^{2+}]_i$ (green fluorescence) by time-lapse confocal microscopy, with the emitted light being separated into green and red using a 565 nm dichroic mirror. For the total ~100 min of time-lapse recordings (see Figs. 1 and 3), focal adjustment of thin confocal sections became necessary, so MTG was co-loaded with the other two fluorescent dyes for this purpose.

The X-Y plane images were 512 by 512 pixels and were taken every 10 sec. Signal increases are presented as the peak/basal fluorescence ratio (F/F_0) and the resting level of the $[O_2^{-\bullet}]_i$ and $[Zn^{2+}]_i$ is $F/F_0=1$ (cf. Fig. 1B).

B. Simultaneous measurement of cytosolic ($[Zn^{2+}]_{cyto}$) and mitochondrial ($[Zn^{2+}]_{mito}$) changes in double-loaded myocytes

RhodZin-3 AM is a red Zn^{2+}-sensitive probe (Kd = 65 nM).[5] When RhodZin-3 AM (568/630 nm BP) is co-loaded with green MTG (488/510 nm; BP), the red fluorescence ($[Zn^{2+}]_{mito}$) can be easily separated from the green MTG by a 565 nm dichroic mirror. Fig. S1A shows an example in which, after one MTG image was saved (the 1st frame in Fig. S1A), the strong excitation green laser line was switched off to preventing photo-damage to the myocytes and the low excitation red laser line was switched on to simultaneously record time-lapse changes in $[Zn^{2+}]_{cyto}$ and $[Zn^{2+}]_{mito}$. For instance, the low red fluorescence in the three mitochondria (3 arrows, 2nd frame) or the nuclei ('N' in the 1st and 2nd frames) was the basal level for the $[Zn^{2+}]_{mito}$ or $[Zn^{2+}]_{cyt}$, respectively. Time-lapse recording of the red fluorescence was then analyzed off-line by locating the MTG (three arrowheads in 1st frame in Fig. S1A) for the $[Zn^{2+}]_{mito}$ and the nuclear region (marked 'N' in the 1st frame) for the $[Zn^{2+}]_{cyto}$.

Intracellular levels of $OH^{\bullet}$ and H_2O_2 were detected using 5-(and–6)-chloromethyl-2',7'-dichlorodihydrofluorescein diacetate acetyl ester (CM-H_2DCFDA). DCFDA is cell-permeable and become highly fluorescent on oxidation by $OH^{\bullet}$ or H_2O_2. Cells were loaded for 60 min at room temperature with 5 μM DCFDA. The excitation/emission wavelengths for DCFDA were 488/540 nm.

Western blot analysis

After treatment, cell lysates prepared by sonication in lysis buffer (60 μg of protein/lane) were immediately electrophoresed on 10 or 12% SDS-PAGE and the proteins transferred to PVDF membrane. Membrane strips were blocked for 1 hour at room temperature with 4% BSA or 5% nonfat milk in Tris-buffered saline (TBS; 150 mM NaCl, 10 mM Tris base, pH 7.4), then incubated with antibodies against phospho-ERK1/2, ERK1/2, phospho-GSK-3β (Ser9), phospho-GSK-3α/β (p-Tyr279)/(p-Tyr216), GSK-3β, p53, Noxa, or Mcl-1 (all 1:500), and antibodies against cleaved caspase-3 (Asp-175) (1:300), PARP (1:1000), or α-tubulin (1:8000) for 16 h at 4°C. After washes with TBS-0.1% Tween, the strips were reacted with horseradish peroxidase-conjugated secondary antibodies (1:1000, PerkinElmer Life Sciences) and visualized using an enhanced chemiluminescence detection system (ECL, PerkinElmer Life Sciences). The density of each band was measured using ImageJ software (NIH, Windows version). The intensity of the band in the vehicle was defined as 100% and the densities of the band in the test sample expressed as a percentage of this value.

Transfection with small interfering RNA (siRNA) and quantitative real-time PCR (qPCR)

siRNA targeting rat GSK-3β (gene designation *Gsk-3β*; gene ID 84027), 12-LOX (gene designation *Alox12*; gene ID 287454), 12/15-LOX (gene designation *Alox15*; gene ID 81639), NFκB p65 (gene designation *Rela*; gene ID 309165), HIF1α (gene designation

Hif1α; gene ID 29560), Noxa (gene designation *Pmaip1*; gene ID 492821), Mcl-1 (gene designation *Mcl-1*; gene ID 60430), p53 (gene designation *Tp53*; gene ID 24842) or Cy3-GAPDH (gene ID 24383) or scrambled siRNA (all siRNAs were 100 nM) was used to transfect myocytes using a low cytotoxicity lipid-based transfection agent, siPORT *NeoFX*. After treatment for 48 hr or 60 hr, whole-cell extracts were prepared and total RNA extracted using RNA-bee (TEL-TEST, TX). cDNA was synthesized from the total RNA in three independent experiments using random primers and High Capacity cDNA Reverse Transcription Kit (Applied Biosystems, CA), according to the manufacture's instructions. qPCR was performed using Power SYBR Green Master Mix and an ABI Prism 7500 Detection System (Applied Biosystems, CA). PCR products were visualized after gel electrophoresis to confirm the presence of a single product of the correct size. The primers used for PCR analysis were: *Gsk-3β* forward, 5'-CTTTGGGATCTGCCATCGA-3', reverse, 5'- GCACTTCCAAAGTCGCAGAGT-3'; *Alox12* forward, 5'-GTTCCGCACATCCGTTACACT-3', reverse, 5'-CCTCC ACCTGTGCTCACTACCT-3'; *Alox15* forward, 5'-GGGCCAGGAGTGACCTGAT-3', reverse, 5'-AAGGCTCCAGCTTGCTTGAG-3; *Rela* forward, 5'-GATCGCCACCGGATTGAAG-3', reverse, 5'- TTCAGTTGGTCCATTGAAAGGA-3; *Hif1a* forward, 5'- TCAGCCAGCAAGTCCTTCTGA-3', reverse, 5'-ATTGACCATATCGCTGTCCACAT-3'; *Pmaip1* forward, 5'-GAACGCGCCATTGAACCCAA-3', reverse, 5'- CTTTGTCTCCAATTCTCCGG-3'; *Mcl-1* forward, 5'- GTAAGGACGAAGCGGGACTG-3', reverse, 5'-AAAAGCCAGCAGCACATTTCT -3'; *Tp53* forward, 5'-TCTGTCATCTTCCGTCCCTTCT-3', reverse, 5'- CGTGCACATAACAGACTTGGCT-3'; *GAPDH* forward, 5'-CGTGTTCCTACCCCCAATGT-3', reverse, 5'-CTCGGCCGCCTGCTT-3'. The level of the test gene was compared to that of the housekeeping gene *GAPDH*. Results are presented as relative gene expression compared to

that of *GAPDH* using $2^{-\Delta\Delta}Ct$.

In situ detection of myocyte apoptosis

(a). cytC release. Cells were fixed, permeabilized, and stained with mouse monoclonal anti-rat cytC antibody (1:500 dilution), followed by FITC-conjugated goat anti-mouse IgG antibody.

(b). Caspase activation. Rabbit polyclonal antibody against cleaved rat caspase-3 (diluted 1:50), which recognizes 17/19 kD activated caspase-3, but not full-length caspase-3 (*i.e.* procaspase-3) or other cleaved caspases, was used. Cells were then labeled for 1 hour at 37°C with FITC-conjugated goat anti-rabbit IgG antibodies

(c). DNA fragmentation (TUNEL) and DNA condensation. DNA fragmentation was detected using the TUNEL method. The TUNEL test was performed following the kit manufacturer's instructions. Nuclear condensation was detected by Hoechst 33342 staining.

Fluorescent images of cytC release, caspase activation, and nuclear condensation were captured and analyzed using a personal computer-controlled charge-coupled device camera and MetaMorph software.

Statistics

All values are presented as mean±SEM of N independent experiments. All data were subjected to one-way ANOVA followed by post hoc test with Bonferroni correction. $P<0.05$ was considered to be statistically significant.

Supplemental Results

Intracellular Zn^{2+} pools are located in both the cytosolic and mitochondrial compartments

Under $Zn^{2+}{}_o$-free conditions, RNS ($ONOO^-$) increased both the $[Zn^{2+}]_{cyto}$ (~9-fold, red line; Figs. S1A-B, S1D) and the $[Zn^{2+}]_{mito}$ (~3-fold, three blue lines; RhodZin-3 measurement; Kd = 65 nM).[5] Compared to the ~9-fold increase in the $[Zn^{2+}]_{cyto}$ measured using RhodZin-3, a much higher (~45-fold) increase was seen using FluoZin-3 (Figs. 1C, F), due to the much lower Kd (~15 nM) of FluoZin-3.[2,5] When TPEN was added during the plateau of the $[Zn^{2+}]_i$ increase (marked post-TPEN, Figs. S1B, S1D), the increases in the $[Zn^{2+}]_{cyto}$ and $[Zn^{2+}]_{mito}$ were both reversed to the basal level within 5 min, indicating that extracellular TPEN can easily penetrate plasmalemma and mitochondrial membranes. Moreover, dithiothreitol (DTT), another membrane-permeating zinc chelator,[6,7] rapidly reversed the H_2O_2-induced $[Zn^{2+}]_i$ increase, but not the $[O_2^{-\bullet}]_i$ increase in FluoZin-3 AM, MitoSox Red, and MTG triple-loaded myocytes (Fig. S1E; cf Fig. 1B).

In neurons, intracellular acidification stimulates $Zn^{2+}{}_i$ release.[5] Rotenone (10 μM, a complex I inhibitor) and FCCP (1 μM, a proton pump inhibitor) both completely depolarized the mitochondrial potential (measured by TMRM), while FCCP, but not rotenone, acidified the pH_i (measured by BCECF, unpublished observations). Rotenone was therefore used to completely depolarize the mitochondrial potential. Figs. S1C-D shows that, upon addition of rotenone, a small transient increase in the $[Zn^{2+}]_{cyto}$ and a simultaneous decrease in the $[Zn^{2+}]_{mito}$ (red arrowhead in Fig. S1C-D) were observed, indicating that mitochondrial depolarization resulted in mitochondrial Zn^{2+} release, which induced a transient increase in the $[Zn^{2+}]_{cyto}$, followed by a decrease. The rapid recovery of the $[Zn^{2+}]_{cyto}$ is probably caused by uptake of Zn^{2+} ions by cytosolic Zn^{2+}-binding proteins (*e.g.* MTs). In the presence of rotenone (Fig. 1C), addition of $ONOO^-$ induced a second large increase in the $[Zn^{2+}]_{cyto}$ and a small increase in the $[Zn^{2+}]_{mito}$ (black arrowhead in Fig.

S1C), probably caused by mitochondrial Zn^{2+} uptake from the markedly increased $[Zn^{2+}]_{cyto}$. This suggests that myocytes have at least two independent $Zn^{2+}{}_i$ storage sites (Figs. S1C-D) and that Zn^{2+} ions can translocate from one to the other.

We next tested whether TPEN chelated Zn^{2+} and not Ca^{2+}. A selective Ca^{2+}-indicator, flow-3 AM, was loaded into myocytes and the experiments were performed in Zn^{2+}-free normal medium (*i.e.* 2 mM $Ca^{2+}{}_o$-containing media). Fig. S1F shows that there was a marked 100 mM KCl-induced $[Ca^{2+}]_i$ increase (100 mM NaCl was replaced by 100 mM KCl). However, addition of TPEN during the plateau of the KCl-induced $[Ca^{2+}]_i$ increase had little effect on the $[Ca^{2+}]_i$ (Fig. S1F). Taken together, these results show that TPEN chelates the $Zn^{2+}{}_i$ increase/release, but not the $Ca^{2+}{}_i$ influx/increase.

At high concentrations (100 μM), baicalein has been suggested to be a potent anti-oxidant which protects against oxidative stress- and I/R-induced myocardial injury.[8,9] DCFDA-loaded myocytes was used to monitor dynamic changes in levels of ROS, including $OH^{\bullet}$ and H_2O_2, and to investigate whether the protective effect of 10 μM baicalein was due to an anti-oxidative effect. Exposure to H_2O_2 or 10 μM Zn^{2+}/K^+ induced a 3- to 4-fold increase in ROS levels (white bars in Fig. S1G). and co-addition of 10 μM baicalein had little effect on ROS production (black bars in Fig. S1G, $p > 0.05$, N=5-6/group).

Intracellular zinc chelation, but not intracellular zinc supplementation ($Zn^{2+}{}_i$ supplement), abolishes oxidative stress- or nitrosative stress-induced nuclear fragmentation and caspase-mediated apoptosis in both cardiomyocytes and cardiac H9c2 myoblasts

Fig. S2 show results for the TUNEL test (A-B) and caspase activation (C) after exposure to simulated I/R, H_2O_2, $ONOO^-$, or $Zn^{2+}{}_i$ supplementation for 4 hr (± inhibitors), followed by return to normal medium for 24 hr.

In cardiomyocytes, I/R- and H_2O_2-induced nuclear fragmentation was markedly

inhibited by TPEN or baicalein (upper and lower panels in Fig. S2A-S2B), again indicating that oxidative stress-induced myocyte apoptosis was inhibited by Zn^{2+}_i chelation or flavonoid. In contrast, after addition of 0.1 μM Zn^{2+}/4 μM pyrithione to the reperfusion solution for only 20 min or co-addition with H_2O_2 for 4 hr, there was little cardioprotection at 24 hr (upper and lower frames in Figs. S2Aiii, S2B). Compared to the response seen at 4 hr (cf. Fig. 2D), the GSK-3 inhibitor SB21 had less protective effect against H_2O_2- or $ONOO^-$-induced nuclear fragmentation and caspase activation at 24 hr (Fig. S2C). However, TPEN, NAC, flavonoids, or U0126 still afforded relative good protection at 24 hr (Fig. S2C) compared to the response at 4 hr (Fig. 2D). These data indicate that Zn^{2+}- and ERK-sensitive, but GSK-3β-insensitive, pathways(s) are involved in H_2O_2-/$ONOO^-$-induced myocyte death (Fig. 8E). Since z-VAD.fmk (a general caspase inhibitor) gave more protection than z-DEVD.fmk (a caspase-3 inhibitor), caspases other than caspase-3 were also activated during the Zn^{2+}_i increase (Fig. S2C). Western blots showed that Zn^{2+}/K^+ induced z-DEVD.fmk- or z-VAD.fmk-sensitive cleavage of both caspase-3 and poly(ADP ribose) polymerase (PARP, Fig. S2D).

Xu and coworkers have demonstrated that, in H9c2 myoblasts, addition of a mixture of 10 μM Zn^{2+} and 4 μM pyrithione to the reperfusion solution for 20 min is cardioprotective.[10] No cell death assay was performed, but they showed that Zn^{2+}_i supplementation increased p-Ser9 levels (GSK3β inhibition) and inhibited 600 μM H_2O_2-induced mitochondrial depolarization at 20 min of reperfusion. However, we found that I/R induced far fewer TUNEL-positive cells at 24 hr using H9c2 cells (Fig. S2B) than using neonatal cultured cardiomyocytes, showing that the cell line was more resistant to I/R treatment. However, when 10 μM Zn^{2+}/4 μM pyrithione was added to the reperfusion solution for 20 min (3rd gray bar in the H9c2 group, Fig. S2B) or was added to the incubation medium for only 20 min (last gray bar in Fig. S2B) or was added with H_2O_2 for 4 hr (lower panel in Fig. S2A; S2B), marked apoptosis was seen at 24 hr.

Persistent TPEN- and U0126-sensitive ERK1/2 phosphorylation induces activation of GSK-3β and Noxa

In cardiomyocytes, treatment with 20 μM Zn^{2+}/100 mM K^+ for 4 hr induced a p-ERK1/2 increase that was TPEN- and U0126-sensitive, but baicalein- and MnTBAP-insensitive (Fig. S3A). Interestingly, when H9c2 cells were used (Fig. S3B) and exposed to a mixture of 10 μM Zn^{2+}/4 μM pyrithione for only 20 min, there was increased phosphorylation of both p-ERK1/2 and p-Ser9 GSK-3β, *i.e.* GSK-3β inhibition (2nd lane in Fig. S3B), confirming the result of Xu and colleagues in H9c2 cells that 10 μM Zn^{2+}/4 μM pyrithione induces an increase in p-Ser9 GSK-3β at ~20 min of treatment.[10] However, we found that, after prolonged Zn^{2+}_i supplementation for 3 hr, there was still a p-ERK increase, but Ser-9 was dephosphorylated, with an increase in p-Tyr216, *i.e.* GSK-3β activation (4th lane in Fig. S3B). Addition of TPEN reversed all the changes in levels of p-ERK and p-GSK-3β at 20 min and at 3 hr (3rd and 5th lanes in Fig. S3B).

Several DNA-damaging agents, including H_2O_2 and cisplatin, induce expression of the apoptotic protein Noxa and degradation of the anti-apoptotic protein Mcl-1, resulting in cell death.[11,12] Using qRT-PCR, we showed that I/R or H_2O_2 induced an increase in Noxa mRNA (Figs. S3C-D) and that U0126 and SB21 abolished the I/R- (Fig. S3C) or the Zn^{2+}/K^+-induced (cf. Fig. 7G) increase in Noxa mRNA levels. We also showed that the endogenous mRNAs, including those for p53, Noxa, or Mcl-1, were knocked down at 48-60 hr after transfection with specific siRNAs in cardiomyocytes (Fig. S3E; cf. Figs. 7E, 8D).

There is evidence that activated GSK-3β phosphorylates Mcl-1 at Ser159, resulting in apoptotic cell death.[13,14] We found that baicalein and SB21 both reversed the Zn^{2+}_i supplement-induced dephosphorylation at Ser9 of GSK-3β, *i.e.* inhibition of GSK-3β activity (cf. Figs. 6B, 6F, 8B, S3F) and that both were cardioprotective (cf. Figs. 2, 4). Since SB21 simultaneously abolished the increase in Noxa expression and Mcl-1

degradation (Figs. 7G, 8B, S3C), we tested whether baicalein had a similar inhibitory effect and found that it also inhibited Noxa expression and Mcl-1 degradation in the presence of Zn^{2+}/K^{+} (Fig. S3F).

Knockdown of LOXs, NFκB or HIF1α does not protect against ROS- or Zn^{2+}/K^{+}-induced caspase-3-dependent myocyte apoptosis

The flavonoids baicalein is known as a potent lipoxygenase (LOX) inhibitor, which shows a protective effect against the ERK-LOX-ROS signaling and abolishes the neuronal Zn^{2+}_{i} toxicity.[15,16] Moreover, oxidative stress is known to activate inflammatory mediators resulting in cell death. Baicalein and luteolin are known to inhibit two inflammatory mediators, including NFκB and HIF1α (induced by ROS).[17,18] Since we observed that baicalein and luteolin exhibited myocyte protection from I/R- and oxidants-induced myocyte apoptosis, these potential targets were knocked down.

qRT-PCR showed that endogenous 12-LOX, 12/15-LOX, NFκB, or HIF1α was markedly knocked down by transfection of myocytes for 48 hr or 60 hr with specific siRNA (Fig. S4A-B). The myocytes remained healthy at 86 hr of transfection of scrambled siRNAs (trypan blue dye exclusion, not shown). However, marked knockdown of 12-LOX and/or 12/15-LOX for 60 hr with specific siRNA (Fig. S4A) did not protect against H_2O_2- or 10 μM Zn^{2+}/K^{+}-induced caspase-3-dependent apoptosis (measured at 86 hr after knockdown the LOXs, Figs. S4C, S4D, S4E), while baicalein (Figs. S4C-S4D) and TPEN (data not shown) remained *protective* against Zn^{2+}-induced myocyte apoptosis, showing that these two LOX proteins are not major targets for flavonoids, which was different as compared with the finding in neurons.[15,19]

We also showed that knockdown of either NFκB or HIF1α had no significant protective effect against ROS-induced apoptosis (Fig. S5A-B), while baicalein, luteolin (Fig. S5C-D) and TPEN (data not shown) remained their protection under these conditions. Thus, none of the four known targets is inhibited by the flavonoids.

Although the time for the turnover of the four proteins is within 2.8-3 hr and more than 75% knockdown of the four mRNAs (qPCR) was seen after the siRNAs treatment for 60 hr (Fig. S4A-B), [18,20] one potential problem in completely excluding the involvement of the four proteins is that we have had no success in measuring the protein levels at 86 hr by Western blot. One possible explanation is that most commercially available antibodies recognize the human, rather than rat, proteins. Since primary rat cardiomyocytes were not healthy after incubation for more than 86 hr, we did not perform the Western blot longer than 86 hr.

Supplemental references

1. Tong H, Imahashi K, Steenbergen C, Murphy E. Phosphorylation of glycogen synthase kinase-3β during preconditioning through a phosphatidylinositol-3-kinase-dependent pathway is cardioprotective. *Circ Res* 2002; **90**: 377–379.
2. Gee KR, Zhou Z-L, Qian WJ, Kennedy R. Detection and imaging of zinc secretion from pancreatic beta-cells using a new fluorescent zinc indicator. *L Am Chem Soc* 2002; **124**: 776-778.
3. Collins TJ, Lipp P, Berridge MJ, Bootman MD. Mitochondrial Ca^{2+} uptake depends on the spatial and temporal profile of cytosolic Ca^{2+} signals. *J Biol Chem* 2001; **276**: 26411–26420.
4. Yang, K-T, Chang, W-L, Yang, P-C, Chien, C-L, Lai, M-S, Su, M-J *et al*. Activation of the transient receptor potential M2 channel and poly(ADP-ribose) polymerase is involved in oxidative stress-induced cardiomyocyte death. *Cell Death Differen* 2006; **13**: 1815-1826.
5. Sensi SL, Ton-That D, Sullivan PG, Jonas EA, Gee KR, Kaczmarek LK *et al*. Modulation of mitochondrial function by endogenous Zn^{2+} pools. *Proc Natl Acad Sci* 2003; **100**: 6157-6162.
6. Cornell NW, Crivaro KE. Stability constant for the zinc-dithiothreitol complex. *Analy Biochem* 1972; **47**: 203-208.
7. Maret W, Vallee BL. Thiolate ligands in metallothionein confor redox activity on Zn^{2+} chelators. *Proc Natl Acad Sci* 1998; **95**: 3478–3482.
8. Shao Z-H, Vanden Hoek TL, Qin Y, Becker LB, Schumacker PT, Li CQ *et al*. Baicalein attenuates oxidant stress in cardiomyocytes. *Am J Physiol* 2002; **282**: H999–H1006.
9. Sadik CD, Sies H, Schewe T. Inhibition of 15-lipoxygenases by flavonoids: structure-activity relations and mode of action. *Biocehm Pharmacol* 2003; **65**: 773–781.
10. Lee SY, Chanoit G, McIntosh R, Zvara DA, Xu Z. Molecular mechanism underlying Akt activation in zinc-induced cardioprotection. *Am J Physiol* 2009; **297**: H569–H575.
11. Aikawa T, Shinzawa K, Tanaka N, Tsujimoto Y. Noxa is necessary for hydrogen peroxide-induced caspase-dependent cell death. *FEBS Letters* 2010; **584**:681–688.
12. Sheridan C, Brumatti G, Elgendy M, Brunet M, Martin SJ. An ERK-dependent pathway to Noxa expression regulates apoptosis by platinum-based chemotherapeutic drugs. *Oncogene* 2010; **29**: 6428-6441.
13. Maurer U, Charvet C, Wagman AS, Dejardin E, Green DR. Glycogen Synthase Kinase-3 Regulates Mitochondrial Outer Membrane Permeabilization and Apoptosis

by Destabilization of MCL-1. *Mol Cell* 2006; **21**: 749–760.

14. Ding Q, He X, Hsu J-M, Xia W, Chen C-T, Li L-Y *et al*. Degradation of Mcl-1 by β-TrCP mediates glycogen synthase kinase 3-induced tumor suppression and chemosensitization. *Mol Cell Biol* 2007; **27**: 4006–4017.
15. Du S, McLaughlin BA, Pal S, Aizenman E. In vitro neurotoxicity of methylisothiazolinone, a commonly used industrial and household biocide, proceeds via a zinc and extracellular signal-regulated kinase mitogen-activated protein kinase-dependent pathway. *J Neurosci* 2002; **22**: 7408–7416.
16. Zhang Y, Wang H, Li J, Jimenez DA, Levitan ES, Aizenman E *et al*. Peroxynitrite-iduced nuronal aoptosis is mediated by intracellular Zinc release and 12-lipoxygenase activation. *J Neurosci* 2004; **24**:10616-10627.
17. Chen C-C, Chow, M-P, Huang W-C, Lin Y-C, Chang Y-J. Flavonoids inhibit tumor necrosis factor-α-induced up-regulation of intercellular adhesion molecule-1 (ICAM-1) in respiratory epithelial Cells through activator protein-1 and nuclear factor-κB: structure-activity relationships. *Mol Pharmacol* 2004; **66**: 683–693.
18. Cho H, Lee HY, Ahn DR, Kim SY, Kim S, Lee KB *et al*. Baicalein induces Functional Hypoxia-Inducible Factor-1α and Angiogenesis. *Mol Pharmacol* 2008; **74**: 70–81.
19. Li Y, Maher P, Schubert D. A role for 12-lipoxygenase in nerve cell death caused by glutathione depletion. *Neuron* 1997; **19**: 453–463.
20. Lawrence T, Bebien M, Liu GY, Nizet V, Karin M. IKKa limits macrophage NF-kB activation and contributes to the resolution of inflammation. *Nature* 2005; **434**: 1138–1143.

Supplemental figure legends

Fig. S1. RNS ($ONOO^-$) induces TPEN-sensitive increases in both the $[Zn^{2+}]_{cyto}$ and $[Zn^{2+}]_{mito}$. **(A-D)** RhodZin3 AM was co-loaded with MTG into cardiomyocytes. Three mitochondria (1-3, 1st frame in A) were analyzed off-line for time-lapse changes in the $[Zn^{2+}]_{mito}$ (three blue lines in B-C), while cytosolic changes in the $[Zn^{2+}]_{cyto}$ were analyzed in the nuclear region (marked N in the 1st frame in A, red line in B-C). Post-treatment with TPEN largely reduces the $ONOO^-$-induced increase in the $[Zn^{2+}]_{cyto}$ and $[Zn^{2+}]_{mito}$ (A-B). Two independent Zn^{2+}_i pools exist in myocytes (C-D). Complete depolarization of the mitochondrial potential by rotenone evokes a small transient increase in the $[Zn^{2+}]_{cyto}$ and a decrease in the $[Zn^{2+}]_{mito}$ (red arrowhead, C-D). Addition of $ONOO^-$ induces a sustained increase in the $[Zn^{2+}]_{cyto}$ and $[Zn^{2+}]_{mito}$ (black arrowhead, C-D). D shows the summarized data from A-C; the data are the mean±SEM, for N =4-6/group. **(E)** DTT (1 mM) rapidly reversed the H_2O_2-induced $[Zn^{2+}]_i$ increase, but not the $[O_2^{-\bullet}]_i$ increase, in triple-loaded myocytes (N=4; cf. Figs. 1B, E-F). **(F)** Fluo-3 AM -loaded cardiomyocytes. KCl (100 mM NaCl was replaced by KCl) induces a TPEN-insensitive $[Ca^{2+}]_i$ increase (N=4). For the concentration of reagents used, see the Supplemental Methods. **(G)** Baicalein (10 μM, black bars) has no inhibitory effect on the H_2O_2- or Zn^{2+}-induced $OH^\bullet$ and H_2O_2 production in cardiomyocytes. Cells were loaded with DCFDA, a ROS (including $OH^\bullet$ and H_2O_2) indicator. The concentrations of H_2O_2 and Zn^{2+}_o (in 100 mM K^+ medium) were 100 μM and 10 μM, respectively. Data are the mean±SEM, N =5-6/group.

Fig. S2. I/R, ROS, RNS, or Zn^{2+}_i supplementation induces TPEN-, NAC-, U0126-, or flavonoid-sensitive DNA fragmentation (TUNEL test) and caspase-dependent myocyte apoptosis. **(A-C)** TPEN, NAC, U0126, or flavonoids inhibit I/R, H_2O_2, $ONOO^-$, or Zn^{2+}/K^+-induced myocyte apoptosis. Cardiomyocytes or H9c2 cells were subjected to I/R, H_2O_2, $ONOO^-$, or Zn^{2+}_i supplement for 4 hr and returned to normal medium for 24 hr. In cardiomyocytes, I/R, H_2O_2, $ONOO^-$, or Zn^{2+}_i supplement induces marked nuclear fragmentation (upper and lower frames in Aii, B) and z-VAD-/caspase-dependent apoptosis at 24 hr (C). TPEN, NAC, or baicalein provides good protection against ROS-/RNS-induced stress, while SB21 only provides slight protection against H_2O_2-/$ONOO^-$-induced apoptosis (A-C). H9c2 cells are more resistant to the I/R treatment (B). Zn^{2+}/pyrithione (added for 20 min) has little protective effect against I/R- or H_2O_2-induced myocyte apoptosis. Moreover, exposure to Zn^{2+}/pyrithione for only 20 min induces marked apoptosis at 24 hr in both H9c2 cells (A-B) and cardiomyocytes (B-C). The data are the mean±SEM, N =6-7/group. **(D)** Western blot analysis. Zn^{2+}/K^+ induces an increase in cleavage of caspase-3 and PARP at 5 hr of exposure. Myocytes were pretreated with z-DEVD.fmk or Z-VAD.fmk (both 100 μM) for 1 hr.

Fig. S3. A sustained increase in Zn^{2+}_i levels activates ERK1/2 and GSK-3β and induces *Noxa* expression. **(A-B)** Twenty μM Zn^{2+}/K^+ was applied to cardiomyocytes in Zn^{2+} free/Ca^{2+}-free/EGTA medium (A) or 10 μM Zn^{2+}/4 μM pyrithione was applied to H9c2 cells in normal medium (B) for the indicated time. TPEN or U0126, but not baicalein or MnTBAP, abolishes the Zn^{2+}_o-induced p-ERK1/2 increase in cardiomyocytes at 4 hr of exposure (A). In H9c2 cells (B), TPEN abolishes the increase in p-ERK and p-Ser9 GSK-3β at 20 min induced by Zn^{2+}/pyrithione. At 3 hr of exposure, TPEN reverses the phosphorylation of p-ERK1/2, dephosphorylation of p-Ser9, and phosphorylation of Tyr216. **(C-E)** qRT-PCR analysis in myocytes. I/R (C) or H_2O_2 (D) exposure induces Noxa mRNA expression. Both U0126 and SB21 inhibit the I/R-induced increase in Noxa mRNA at 5 hr of treatment (C). Expression of endogenous mRNAs (p53, Noxa, or Mcl-1) determined by qRT-PCR after treatment with the indicated siRNAs. mRNAs were knocked down by transfection with sip53, siNoxa, or siMcl-1 for 48 or 60 hr. N=3-4/group (E). **(F)** Western blot analysis in myocytes. Baicalein simultaneously abolished the Zn^{2+}/K^+-induced p-Ser9 dephosphorylation, the increase in Noxa protein levels, and the decrease in Mcl-1 protein levels (cf. Fig. 8B).

Fig. S4. Knockdown of LOXs does not protect against ROS- and Zn^{2+}_o-induced myocyte apoptosis. **(A-B)** Expression of 12-LOX or 12/15-LOX **(**A**)** or NFκB or HIF1α **(**B**)** in myocytes determined by qRT-PCR after treatment with the indicated siRNAs. The graphs shows expression expressed as a fold change compared to expression using scrambled siRNA. Significant differences in expression are indicated as $^*p<0.05$ *vs* scrambled siRNA group. **(C-E)** H_2O_2- and 10 μM Zn^{2+}/40 mM K^+-induced caspase-dependent nuclear condensation was not inhibited by transfection with si12-LOX (C), si12/15-LOX (D) or si12-LOX plus si12/15-LOX (E), while the Zn^{2+}_o-induced apoptosis is inhibited by baicalein (± siRNAs; 'bai', summarized data in C-E). Little caspase activation and nuclear condensation are seen when scrambled siRNA (first frames, C-E) or baicalein (the last frame in C-D) is used.

Fig. S5. H_2O_2- and Zn^{2+}_o-induced myocyte apoptosis is not inhibited by knockdown of NFκB (A, C) or HIF1α (B, D). The 10 μM Zn^{2+} increase-induced apoptosis is again inhibited by baicalein or leuteolin [both 10 μM ± siRNAs; $^*p<0.05$ compared to Zn^{2+}+siNFκB group (C) or to Zn^{2+}+siHIF1α group (D)]. Little caspase activation and nuclear condensation are seen when scrambled siRNA is used (first frames of A-B).

Fig. S1

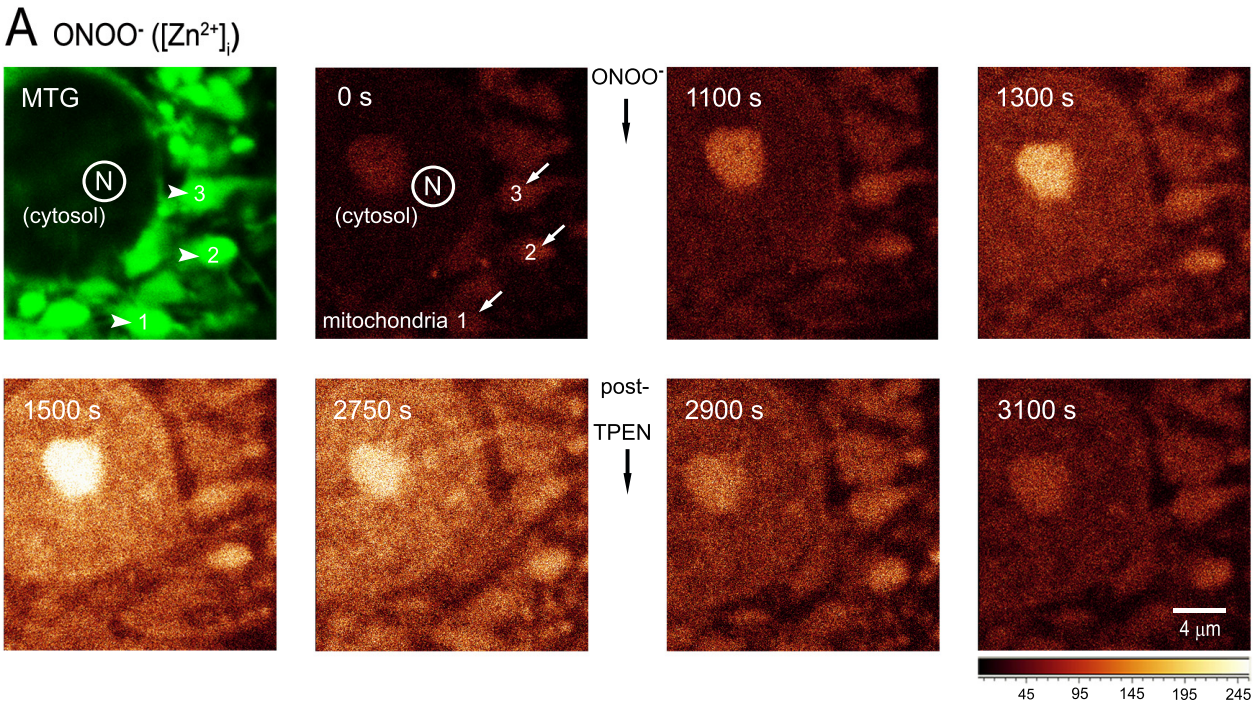
A ONOO- ([Zn2+]i)
MTG
N
(cytosol)
3
2
1
0 s
mitochondria 1
ONOO-
1100 s
1300 s
1500 s
2750 s
post-
TPEN
2900 s
3100 s
4 μm
45
95
145
195
245

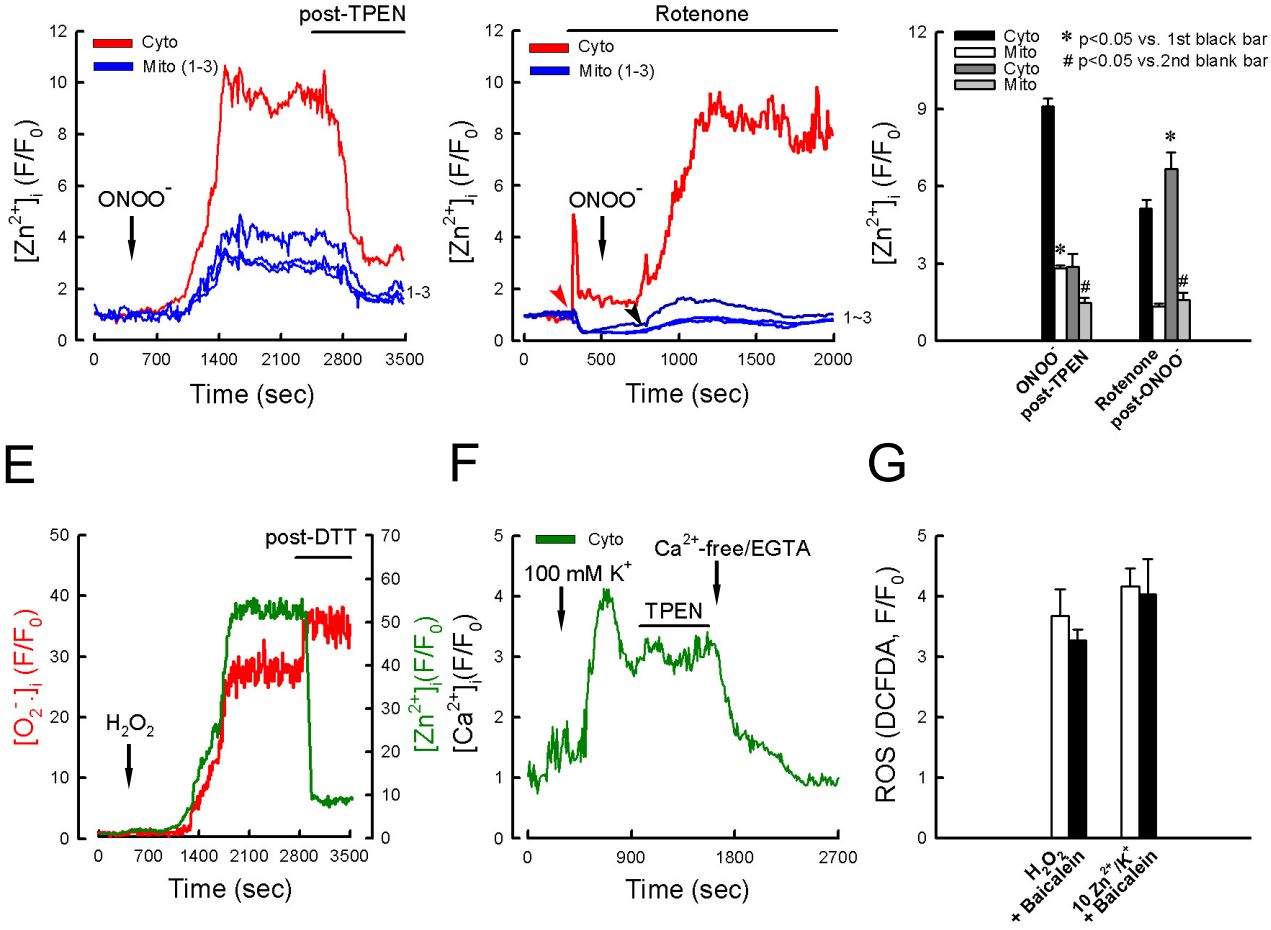
B
post-TPEN
Cyto
Mito (1-3)
ONOO-
1-3
[Zn2+]i (F/F0)
Time (sec)
C
Rotenone
Cyto
Mito (1-3)
ONOO-
1~3
[Zn2+]i (F/F0)
Time (sec)
D
Cyto
Mito
Cyto
Mito
* p<0.05 vs. 1st black bar
# p<0.05 vs.2nd blank bar
[Zn2+]i (F/F0)
ONOO-
post-TPEN
Rotenone
post-ONOO-
E
post-DTT
H2O2
[O2-·]i (F/F0)
[Zn2+]i(F/F0)
Time (sec)
F
Cyto
100 mM K+
Ca2+-free/EGTA
TPEN
[Ca2+]i(F/F0)
Time (sec)
G
ROS (DCFDA, F/F0)
H2O2
+ Baicalein
10 Zn2+/K+
+ Baicalein

Fig. S2

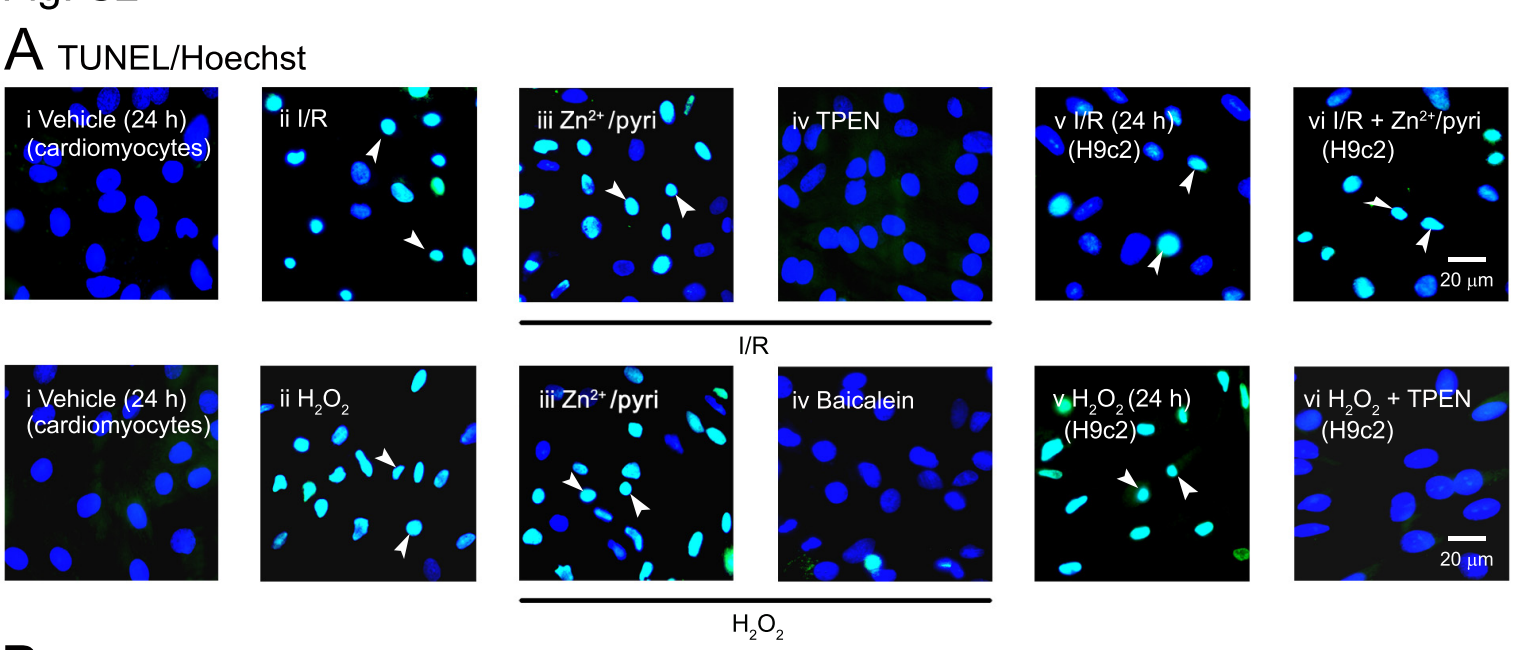
A TUNEL/Hoechst
i Vehicle (24 h) (cardiomyocytes)
ii I/R
iii Zn2+ /pyri
iv TPEN
v I/R (24 h) (H9c2)
vi I/R + Zn2+/pyri (H9c2)
20 μm
I/R
i Vehicle (24 h) (cardiomyocytes)
ii H2O2
iii Zn2+ /pyri
iv Baicalein
v H2O2 (24 h) (H9c2)
vi H2O2 + TPEN (H9c2)
20 μm
H2O2

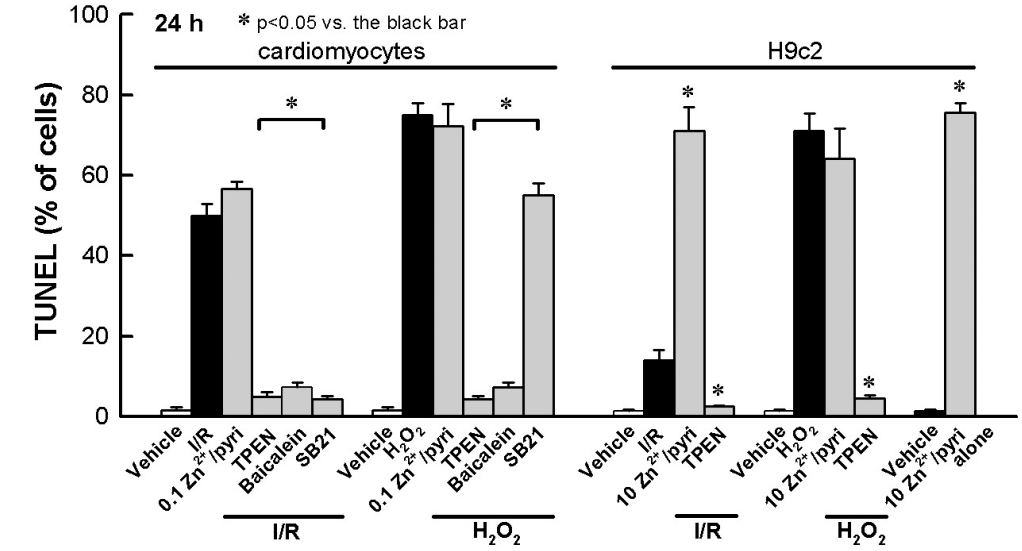
B
24 h
* p<0.05 vs. the black bar
cardiomyocytes
H9c2
TUNEL (% of cells)
Vehicle
I/R
0.1 Zn2+/pyri
TPEN
Baicalein
SB21
H2O2
10 Zn2+/pyri
alone
I/R
H2O2

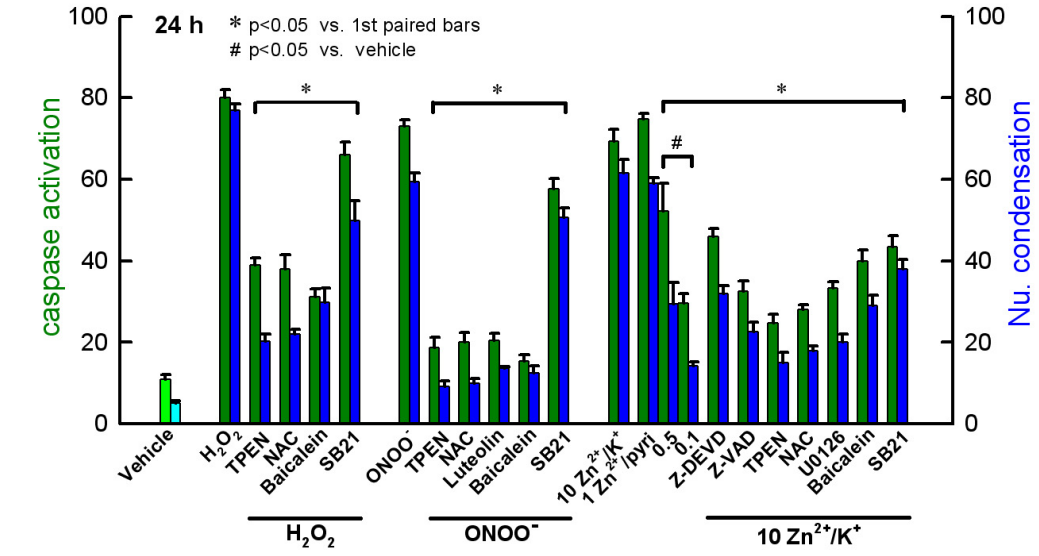
C
24 h
* p<0.05 vs. 1st paired bars
# p<0.05 vs. vehicle
caspase activation
Nu. condensation
Vehicle
H2O2
TPEN
NAC
Baicalein
SB21
ONOO-
Luteolin
10 Zn2+/K+
1 Zn2+/pyri
0.5
0.1
Z-DEVD
Z-VAD
U0126
H2O2
ONOO-
10 Zn2+/K+

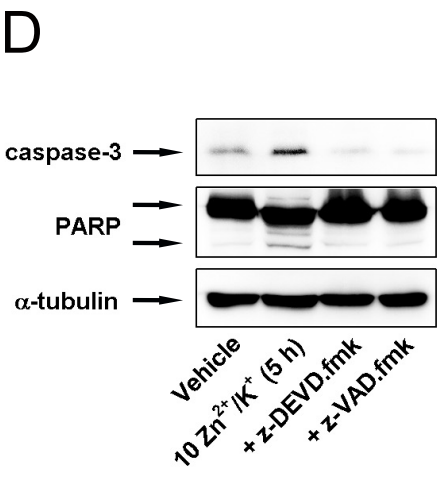
D
caspase-3
PARP
α-tubulin
Vehicle
10 Zn2+/K+ (5 h)
+ z-DEVD.fmk
+ z-VAD.fmk

Fig. S3

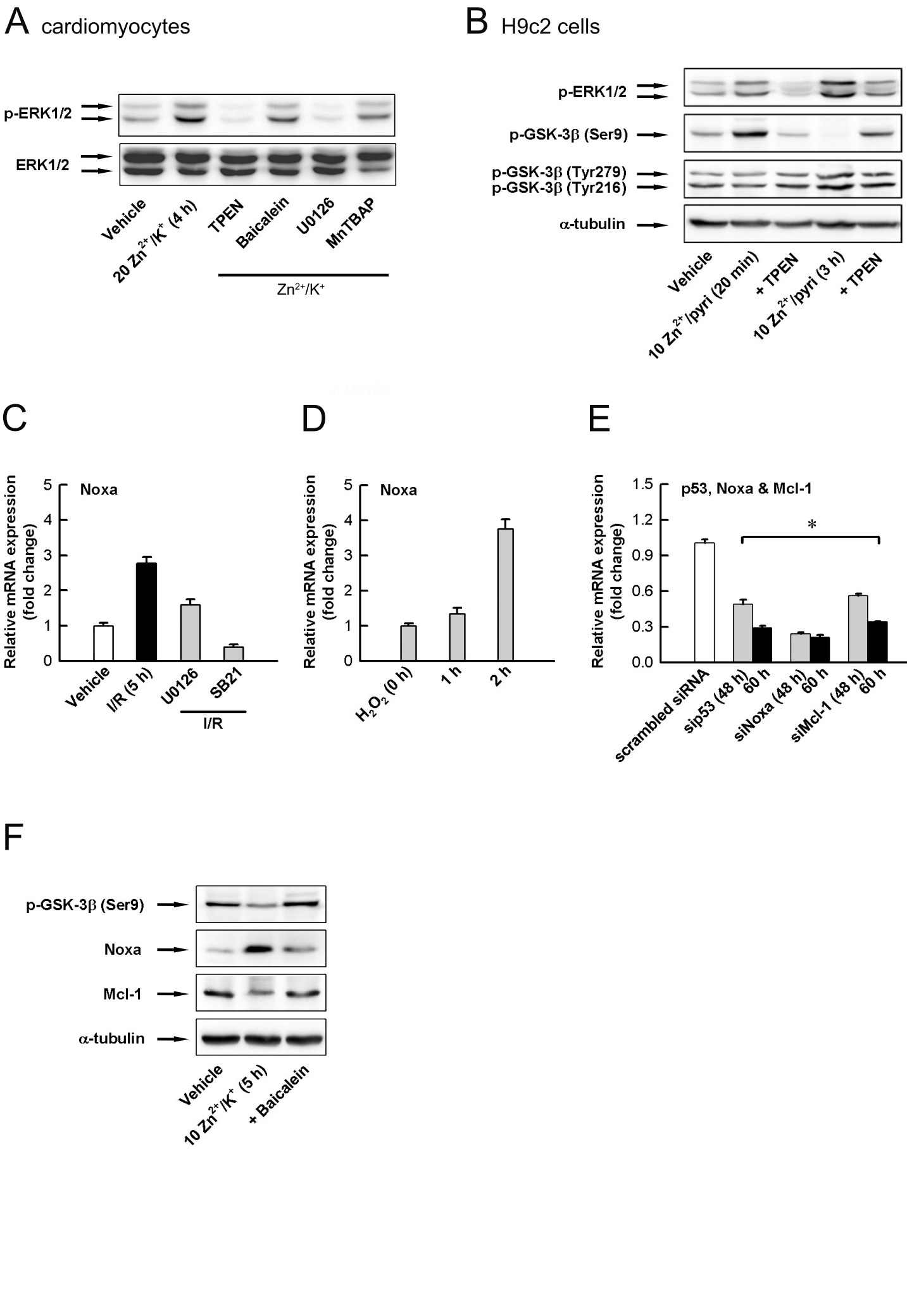
A cardiomyocytes
p-ERK1/2
ERK1/2
Vehicle
20 Zn2+/K+ (4 h)
TPEN
Baicalein
U0126
MnTBAP
Zn2+/K+
B H9c2 cells
p-ERK1/2
p-GSK-3β (Ser9)
p-GSK-3β (Tyr279)
p-GSK-3β (Tyr216)
α-tubulin
Vehicle
10 Zn2+/pyri (20 min)
+ TPEN
10 Zn2+/pyri (3 h)
+ TPEN
C
Noxa
Relative mRNA expression (fold change)
Vehicle
I/R (5 h)
U0126
SB21
I/R
D
Noxa
Relative mRNA expression (fold change)
H2O2 (0 h)
1 h
2 h
E
p53, Noxa & Mcl-1
Relative mRNA expression (fold change)
*
scrambled siRNA
sip53 (48 h)
60 h
siNoxa (48 h)
60 h
siMcl-1 (48 h)
60 h
F
p-GSK-3β (Ser9)
Noxa
Mcl-1
α-tubulin
Vehicle
10 Zn2+/K+ (5 h)
+ Baicalein

Fig. S4

A

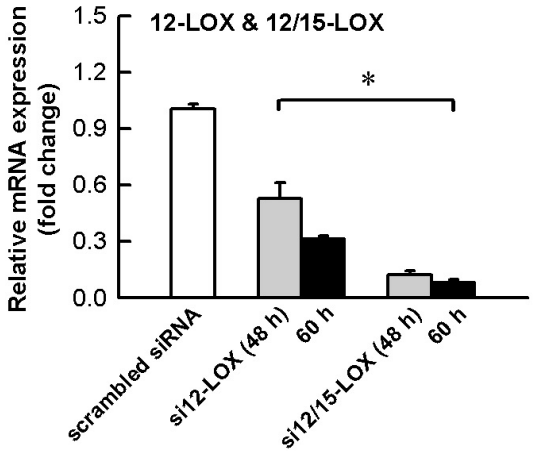

B

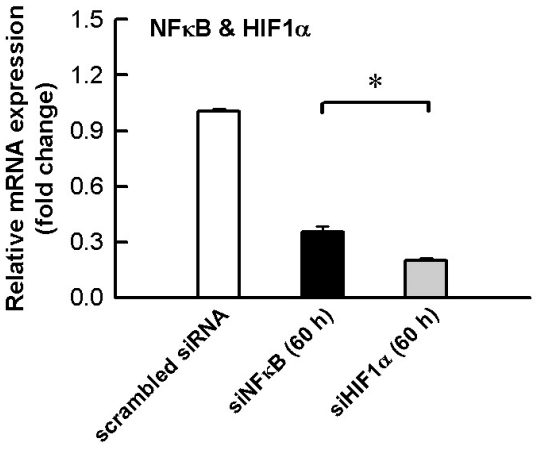

C si12-LOX

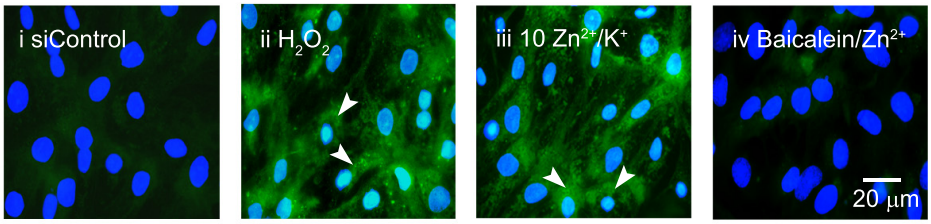

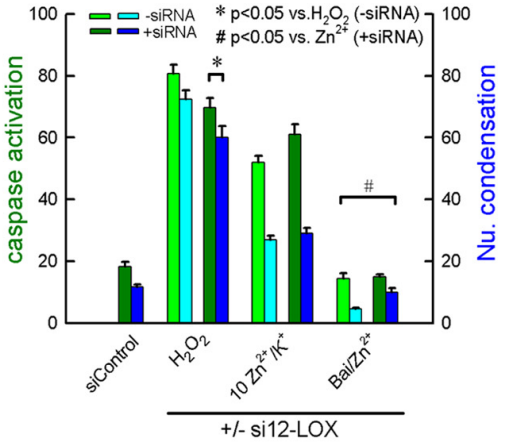

D si12/15-LOX

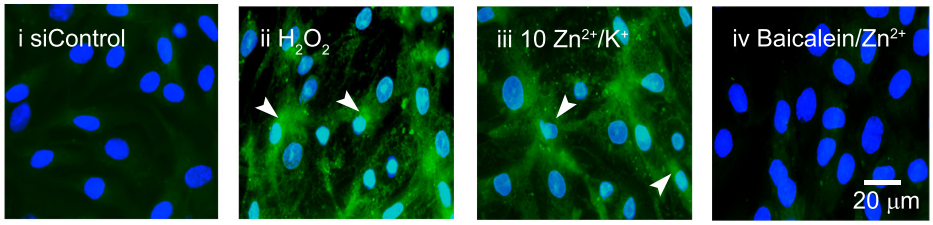

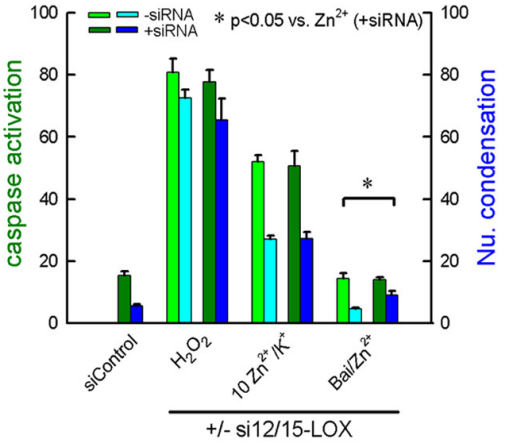

E si12-LOX & si12/15-LOX

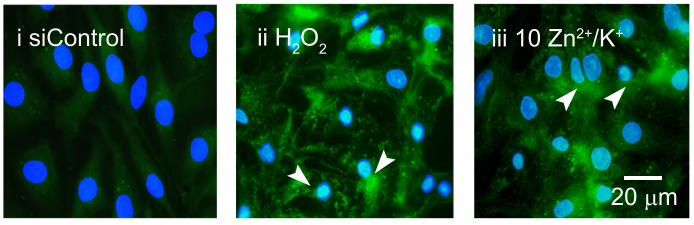

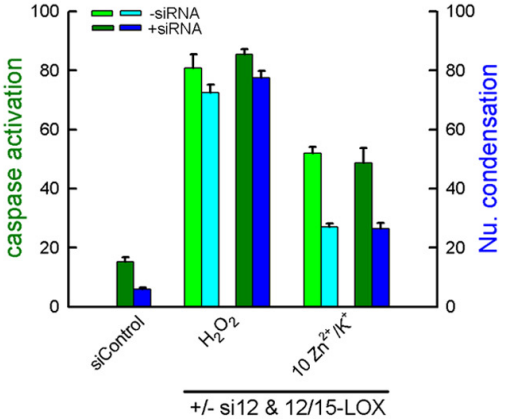

Fig. S5

A siNFκB

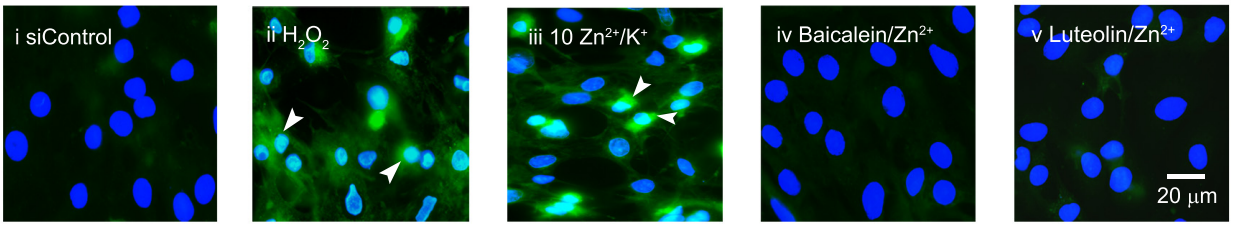

B siHIF1α

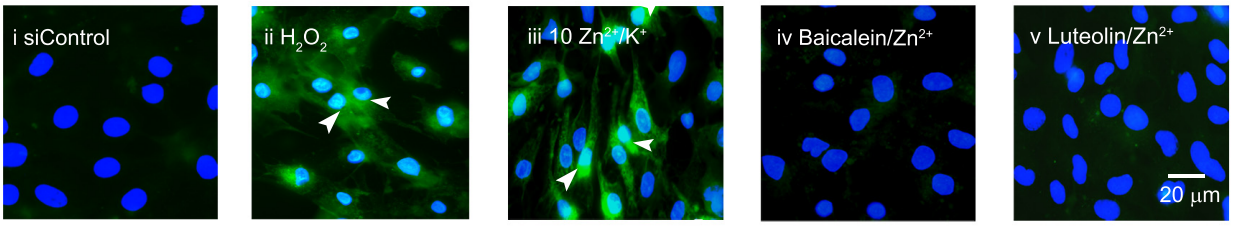

C

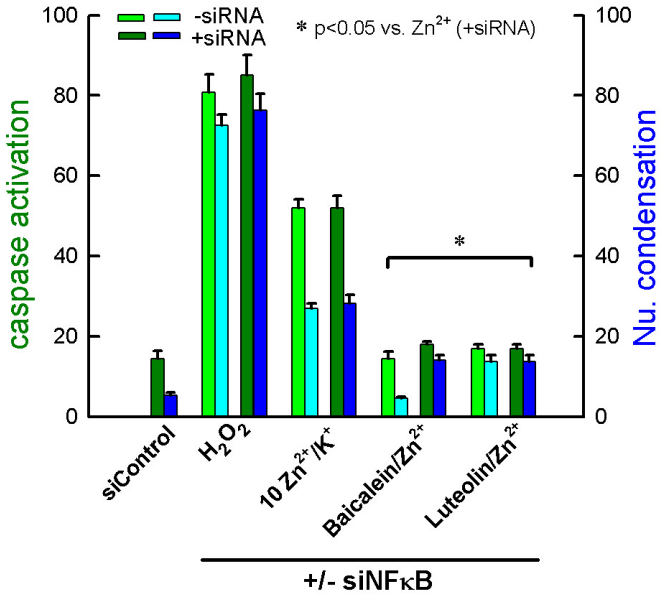

D